

# Circumstantial Evidence for Rotating Mass Matrix from Fermion Mass and Mixing Data

José BORDES

jose.m.bordes @ uv.es

*Departament Fisica Teorica, Universitat de Valencia,  
calle Dr. Moliner 50, E-46100 Burjassot (Valencia), Spain*

CHAN Hong-Mo

chanhm @ v2.rl.ac.uk

*Rutherford Appleton Laboratory,  
Chilton, Didcot, Oxon, OX11 0QX, United Kingdom  
and*

*NAPL, Department of Physics,*

*University of Oxford, Oxford, United Kingdom*

TSOU Sheung Tsun

tsou @ maths.ox.ac.uk

*Mathematical Institute, University of Oxford,  
24-29 St. Giles', Oxford, OX1 3LB, United Kingdom*

## Abstract

It is shown that existing data on the mixing between up and down fermion states and on the hierarchical mass ratios between fermion generations, as far as can be so analysed at present, are all consistent with the two phenomena being both consequences of a mass matrix rotating in generation space with changing energy scale. As a result, the rotating mass matrix can be traced over some 14 orders of magnitude in energy from the mass scale of the  $t$ -quark at 175 GeV to below that of the atmospheric neutrino at 0.05 eV.

# 1 Introduction

Along with the mystery of why there should be in nature 3, and apparently only 3, generations of fermions, the fact that their masses should be hierarchical and that they should mix, as embodied for quarks in the CKM matrix [1] and exhibited for leptons in neutrino oscillations, has remained one of the great puzzles of particle physics. In the context of what we call the Dualized Standard Model (DSM) [2] which is an explicit attempt to solve this generation puzzle, we have suggested that the mass hierarchy and the mixing phenomenon can both result from a mass matrix which changes its orientation in generation space (rotates) with changing energy scales and have obtained rather good agreement with experiment based on this hypothesis. This previous treatment however depends first on the details of the DSM mechanism driving the rotation which we suspect are not strictly necessary for deriving the said result, and secondly, it does not clearly reveal the degree of significance of the claimed agreement with experiment nor the amount of direct empirical support, if any, for mass matrix rotation. For this reason, our purpose in this paper is to turn the argument around by going straight to the experimental data and seek evidence there for the rotation hypothesis.

Our strategy is as follows. We shall keep the previous assumption that both mass hierarchy and mixing arise from mass matrix rotation (with the rotation being a fairly smooth function of scale), but instead of seeking as we did to deduce the mass and mixing parameters from a prescribed rotation curve, we shall use the existing data to determine the rotation required at each scale to reproduce the observed range of values for these parameters. We shall show that by inputting all the available mass and mixing data on both quarks and leptons, one can trace the implied rotation over a scale range of some 14 orders of magnitude. The result is seen to be all quite consistent with the fermions lying on a single smooth rotation curve linking the  $t$  quark at 175 GeV through all the intermediate fermion states down to the second heaviest neutrino  $\nu_2$  at less than  $10^{-2}$  eV. Moreover, the shape of this curve is indicative of certain features previously predicted by the DSM calculation, such as the two rotational fixed points at infinite and zero energies. We consider these results as positive evidence for mass matrix rotation.

The evidence, however, is at present only circumstantial because it relies on the ansatz that mass hierarchy and mixing arise as consequences of mass matrix rotation, made on the premises that these phenomena would otherwise be hard to explain. Let us begin then by re-examining the reasoning behind this ansatz. That a rotation of the mass matrix with changing scales will

automatically lead to mixing and a hierarchical mass spectrum is most easily seen in the simplified scenario when there are only 2 generations instead of 3, which is in fact not a bad approximation in the high energy region comprising all fermions with masses down to  $m_\mu \sim 100$  MeV. In this scenario, suppose the mass matrices for up and down states are aligned in orientation and that each has only one massive eigenstate. Then in the absence of mass matrix rotation, one concludes that there is no mixing and that the lower generation states are massless. However, if the mass matrix rotates, the above conclusion will no longer be true. The point is that once the mass matrix rotates with changing scale, then even the usual definition of flavour states as its eigenstates will have to be refined since the eigenstates depend now also on the scale. For example, in defining the state vector  $\mathbf{v}_t$  of  $t$  as the massive eigenstate of the  $U$ -quark mass matrix it has now to be specified that it is to be taken at the scale  $\mu = m_t$ . At this scale, we have then the situation depicted in Figure 1, where  $c$ , being by definition an independent quantum state to  $t$ , is necessarily represented by the vector  $\mathbf{v}_c$  orthogonal to  $\mathbf{v}_t$  and has thus by assumption a zero eigenvalue. But this should not be interpreted to mean that  $c$  has a zero mass, for this eigenvalue is evaluated at the scale  $\mu = m_t$  whereas the mass of  $c$  should be evaluated instead at the scale  $\mu = m_c$ . Given now that the mass matrix rotates with changing scales, its massive eigenvector will have rotated already by the scale  $\mu = m_c$  to a different direction as seen in Figure 1 and acquired a component in the direction of  $\mathbf{v}_c$ , hence giving  $c$  by “leakage” a nonzero mass:

$$m_c = m_t \sin^2 \theta_{tc}, \quad (1)$$

with  $\theta_{tc}$  being the rotation angle between the scales  $\mu = m_t$  and  $\mu = m_c$ . Similarly, one sees from Figure 2 that by virtue of the rotation from the scale  $\mu = m_t$  to the scale  $\mu = m_b$  where the state vector  $\mathbf{v}_b$  is defined, there will be mixing between the  $t$  and  $b$  states with the CKM matrix element:

$$V_{tb} = \mathbf{v}_t \cdot \mathbf{v}_b = \cos \theta_{tb} \neq 1. \quad (2)$$

where  $\theta_{tb}$  is the rotation angle between the two scales. Hence, already from these examples, one sees that both lower generation masses and nontrivial mixing will automatically be obtained from a rotating mass matrix even if one starts with neither. It seems thus natural to entertain as we did above the possibility that this is indeed how the fermion mass hierarchy and the fermion mixing arise, given that one has otherwise no generally accepted explanation as yet for these phenomena.

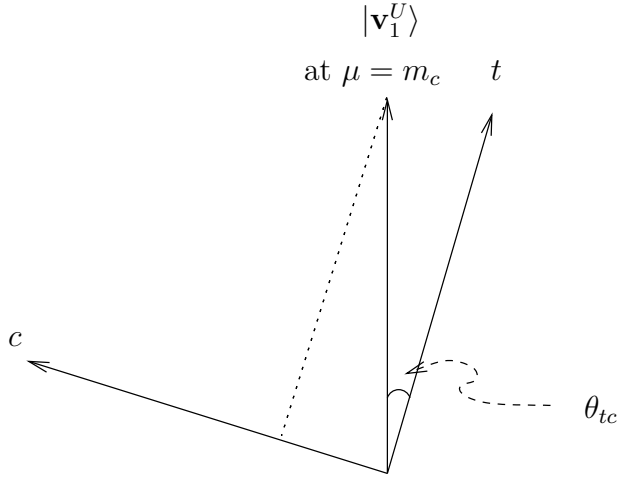


Figure 1: Masses for lower generation fermions from a rotating mass matrix via the “leakage” mechanism.

Our aim then in this paper is to seek evidence from existing fermion mass and mixing data for the preceding proposition. This is not hard to do if there were indeed only two generations of fermions, for in that case the rotation angle is additive and the angle between different mass scales can be read off directly from the mass ratios between fermion generations and the mixing angles between up and down fermion states via respectively (1) and (2). Even when there are 3 generations but with the problem remaining approximately planar, as is actually the case for mass ratios and most of the mixing angles at scales above  $m_\mu \sim 100$  MeV, the same simple analysis applies. This has been done in [3] using the experimental data in [4] and gives the Figure 3, where one sees that the empirical points with the errors shown already suggest by themselves a rotation similar to that proposed earlier by our DSM calculation. Indeed, making a best fit with the data by MINUIT produces a curve

$$\theta = \exp(-2.267 - 0.509 \ln \mu) - 0.0075, \text{ for } \mu \text{ in GeV,} \quad (3)$$

with a  $\chi^2$  of 0.21 per degree of freedom which is hardly distinguishable from the DSM curve calculated two years before in [5], as can be seen in the same figure. We regard this preliminary agreement as already a nontrivial support for the rotation hypothesis. In particular one notes that the data are indicative of the rotation angle approaching an asymptotic value thus suggesting a fixed point at infinite scale as predicted by the DSM.

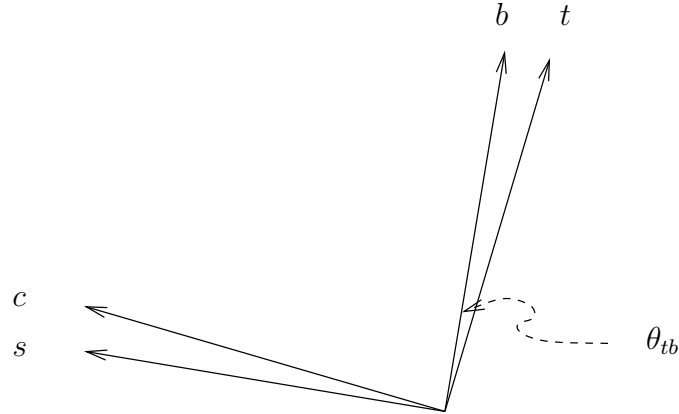


Figure 2: Mixing between up and down fermions from a rotating mass matrix.

The above analysis, however, is incomplete in that it relies on the planar approximation and is restricted for that reason only to scales above the  $\mu$  mass. To test the rotation hypothesis exhaustively against existing data, these restrictions will have to be removed to ensure that no hidden violation of the hypothesis exists for the full rotation in 3-dimensional generation space, or for scales further down where the planar approximation no longer applies. At first we thought this was not possible with the present available data, but later found a method of analysis whereby the difficulties previously encountered could be overcome, as we shall detail below.

We note first that starting with the same assumption as before that the nonzero masses for lower generations arise just from mass matrix rotation, it follows that the now  $3 \times 3$  mass matrix still has at any scale only one massive eigenvector which changes its direction with changing scales, thus tracing out a trajectory on the unit sphere in 3-dimensional generation space. The whole content of the rotating mass matrix is thus encapsulated in the rotation of this single vector  $\mathbf{r}(\mu)$  depending on scale  $\mu$ , and the main technical problem posed by the present analysis is just how to extract this vector at various scales from the existing data on fermion mass ratios and mixing parameters. Once so extracted, the vector can then be confronted with the rotation hypothesis and should be consistent with tracing out a continuous curve in 3-space if the hypothesis is correct. For the extraction of this vector, we proceed now as follows.

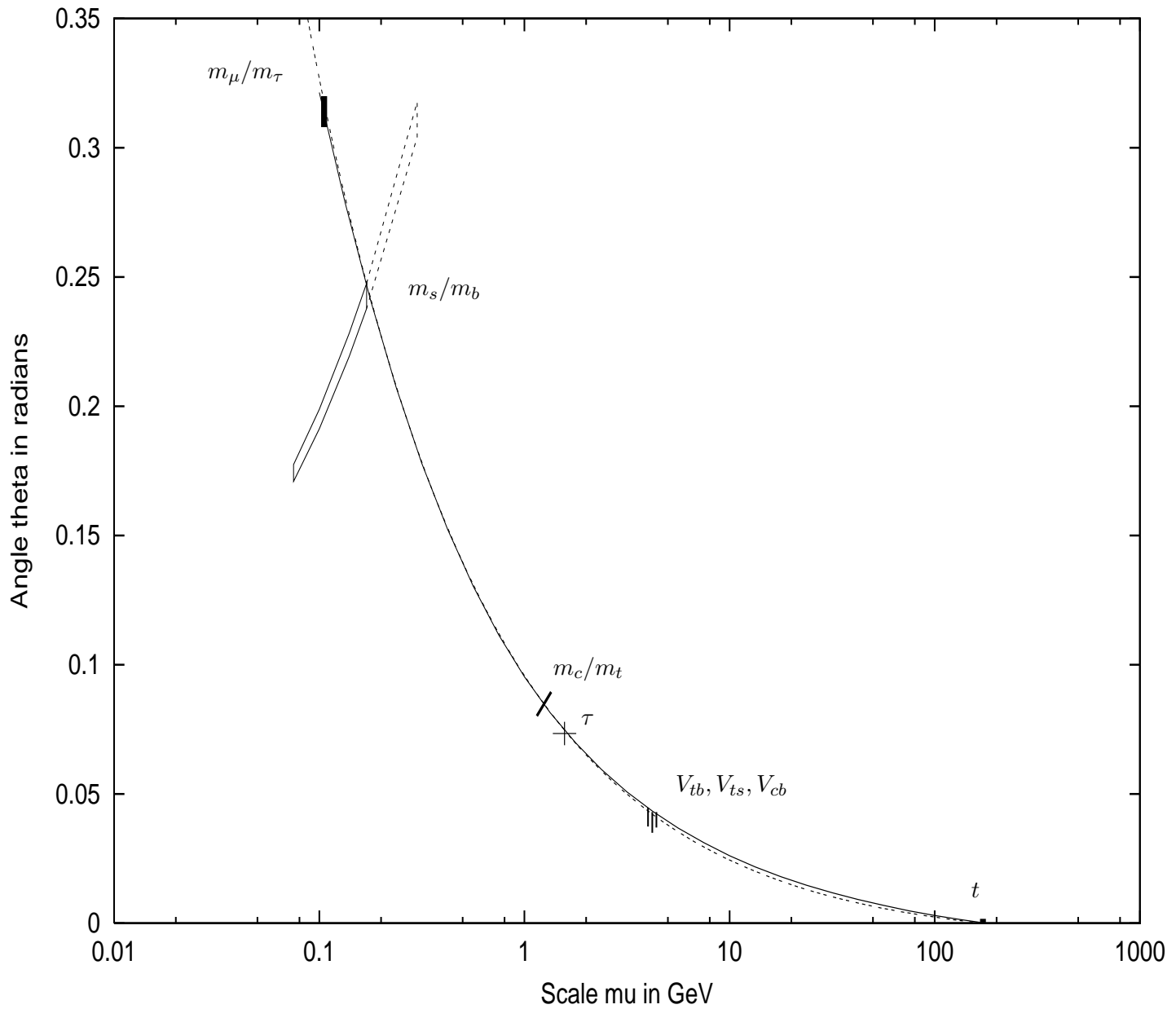


Figure 3: The rotation angle changing with scale as extracted from data on mass ratios and mixing angles and compared with the best fit to the data (dashed curve) and the earlier calculation by DSM (full curve) [5], in the planar approximation.

## 2 Extracting $\mathbf{r}(\mu)$ from quark data

The  $U$ -quarks  $t, c, u$  are independent quantum states so that their state vectors should form an orthonormal triad in generation space, which we can choose without loss of generality as:

$$\mathbf{v}_t = (1, 0, 0); \quad \mathbf{v}_c = (0, 1, 0); \quad \mathbf{v}_u = (0, 0, 1). \quad (4)$$

The  $D$ -quark state vectors also form an orthonormal triad the orientation of which relative to the  $U$ -triad is given by the CKM matrix elements:

$$\mathbf{v}_b = (V_{tb}, V_{cb}, V_{ub}); \quad \mathbf{v}_s = (V_{ts}, V_{cs}, V_{us}); \quad \mathbf{v}_d = (V_{td}, V_{cd}, V_{ud}). \quad (5)$$

Hence, if the complex elements of the CKM matrix are accurately known, the  $D$ -triad would also be determined. At present, however, only the absolute values of the CKM matrix elements are experimentally known to reasonable accuracy, leading thus to some ambiguities in the determination of the  $D$ -triad. In particular, one is forced to ignore for the moment in the CKM matrix the CP-violating phase which is experimentally very poorly determined and treat the  $D$ -triad also as real vectors. Inserting then the experimental limits on the CKM matrix elements as read from [4] gives rather tight constraints on the directions of the  $D$ -triad with errors so small as to be mostly negligible for our analysis:

$$\begin{aligned} \mathbf{v}_b &= ((0.9990 - 0.9993), (0.037 - 0.043), -(0.002 - 0.005)); \\ \mathbf{v}_s &= (-(0.035 - 0.043), (0.9734 - 0.9749), (0.219 - 0.226)); \\ \mathbf{v}_d &= ((0.004 - 0.014), -(0.219 - 0.225), (0.9742 - 0.9757)). \end{aligned} \quad (6)$$

The signs of the 3 components for  $b$  can be chosen arbitrarily by choosing the physically irrelevant phases of the various quark state vectors and a particular choice has been made in (6) for convenience. The signs for the other 2 states are then determined by orthogonality. Actually, given the present errors on the CKM matrix elements, there is an alternative solution to that shown for the state vectors of  $s$  and  $d$ , which however we disfavour for reasons of continuity to be explained below.

We notice that by the considerations in the preceding section, the state vector of  $b$ , this being the heaviest state in the  $D$  sector, is just the rotating vector  $\mathbf{r}(\mu)$  taken at the scale  $\mu = m_b$ , thus:

$$\mathbf{r}(m_b) = \mathbf{v}_b. \quad (7)$$

Together with:

$$\mathbf{r}(m_t) = \mathbf{v}_t = (1, 0, 0), \quad (8)$$

we have then two points on the trajectory for  $\mathbf{r}(\mu)$  we wish to trace. One convenient way to present this, we find, is to write this rotating vector as  $\mathbf{r}(\mu) = (\xi(\mu), \eta(\mu), \zeta(\mu))$  with  $\xi(\mu)^2 = 1 - \eta(\mu)^2 - \zeta(\mu)^2$  and plot the constraints on  $\eta(\mu)$  and  $\zeta(\mu)$  on the  $\eta\zeta$ -plane. The result from (8) and (7) are then entered as the first 2 points from the left in the 3-D plot of Figure 4. This plot, which shows  $\eta(\mu)$  and  $\zeta(\mu)$  as functions of the energy scale  $\mu$  can in principle incorporate all the information that we shall extract from data. However, it being often hard to read the information it contains, we shall supplement it by its 3 projections onto the 3 co-ordinate planes, namely onto the  $\eta\zeta$ -plane in Figure 5, the  $\mu\eta$ -plane in Figure 6, and the  $\mu\zeta$ -plane in Figure 7, which projections, as we shall see, will be useful later also for interpolation and extrapolation purposes.

Next, we turn to consider  $\mathbf{r}(\mu)$  at the scale  $\mu = m_c$ . Since the mass of  $m_c$ , by our original hypothesis, comes about only through the “leakage” from  $m_t$  as detailed above, it follows that the vector  $\mathbf{r}(m_c)$  will have to be a linear combination:  $\cos \theta_{tc} \mathbf{v}_t + \sin \theta_{tc} \mathbf{v}_c$ , of the state vectors  $\mathbf{v}_t$  and  $\mathbf{v}_c$  of respectively  $t$  and  $c$  with  $\sin \theta_{tc}$  given by (1), or explicitly:

$$\mathbf{r}(m_c) = \sqrt{1 - m_c/m_t} \mathbf{v}_t + \sqrt{m_c/m_t} \mathbf{v}_c. \quad (9)$$

Inputting the experimental limits  $m_t = 174.3 \pm 5.1$  GeV and  $m_c = 1.15 - 1.35$  GeV from [4] then gives us the allowed region for the third data point on the trajectory of  $\mathbf{r}(\mu)$ , as is shown on Figure 4. There is in fact of course another solution for  $\mathbf{r}(m_c)$  in (9) with  $\sin \theta_{tc}$  taking the value  $-\sqrt{m_c/m_t}$ , but this we discard for reasons of continuity. Such an ambiguity will in fact always occur for all the other pieces of information on  $\mathbf{r}(\mu)$  we shall extract from data, since experiment so far gives only the absolute values of the relevant quantities, but the ambiguity can almost always be resolved by a similar appeal to continuity as above.

The next point in line is  $\mathbf{r}(\mu)$  at  $\mu = m_s$ , which will of necessity be poorly determined because the  $s$  mass is very poorly known. Nevertheless, whatever is taken for the mass of  $s$  so long as it is given by the “leakage mechanism” from  $b$ ,  $\mathbf{r}(m_s)$  will have to be a linear combination of the state vector  $\mathbf{v}_b$  of  $b$  and the state vector  $\mathbf{v}_s$  of  $s$ , so that by reasoning exactly as above for  $c$ , we have:

$$\mathbf{r}(m_s) = \sqrt{1 - m_s/m_b} \mathbf{v}_b + \sqrt{m_s/m_b} \mathbf{v}_s. \quad (10)$$

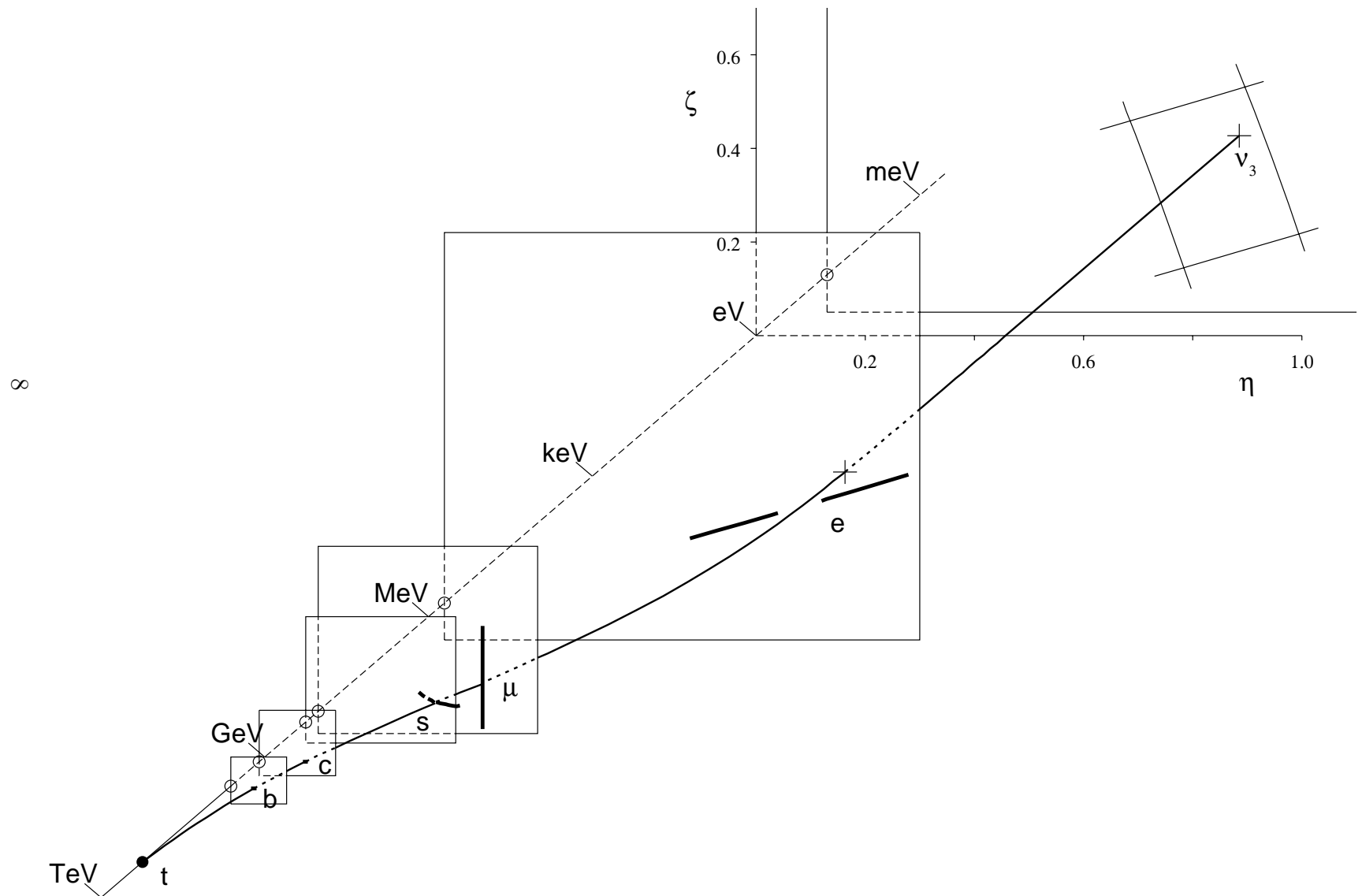


Figure 4: A plot of the rotating vector  $\mathbf{r}(\mu)$  as extracted from existing data on fermion mass ratios and mixing parameters, where its second and third components, i.e.  $\eta(\mu)$  and  $\zeta(\mu)$ , are plotted as functions of  $\ln \mu$ ,  $\mu$  being the energy scale. The experimentally allowed values at any one scale are represented as an allowed region on a plaquette, with the scale corresponding to a plaquette being given by the intersection, denoted by a small circle, of its left-most boundary with the  $\mu$ -axis. For example, the first small plaquette on the left of the figure corresponds to the scale  $\mu = m_b$ , on which plaquette the allowed region for  $\mathbf{r}(\mu) = \mathbf{v}_b$  is very small because of the small experimental error on the CKM matrix elements  $V_{tb}, V_{cb}$  and  $V_{ub}$ . The last plaquette on the right, on the other hand, corresponds to the scale  $\mu = m_{\nu_3}$ , on which plaquette the allowed region for  $\mathbf{r}(\mu)$  is a rough rectangular area bounded by the data on  $\nu$  oscillations from atmospheric neutrinos and from the Chooz experiment. The curve represents the result of a DSM one-loop calculation from an earlier paper [5] which is seen to pass through the allowed region on every plaquette except that for the electron  $e$ . For further explanation of details, please see text.

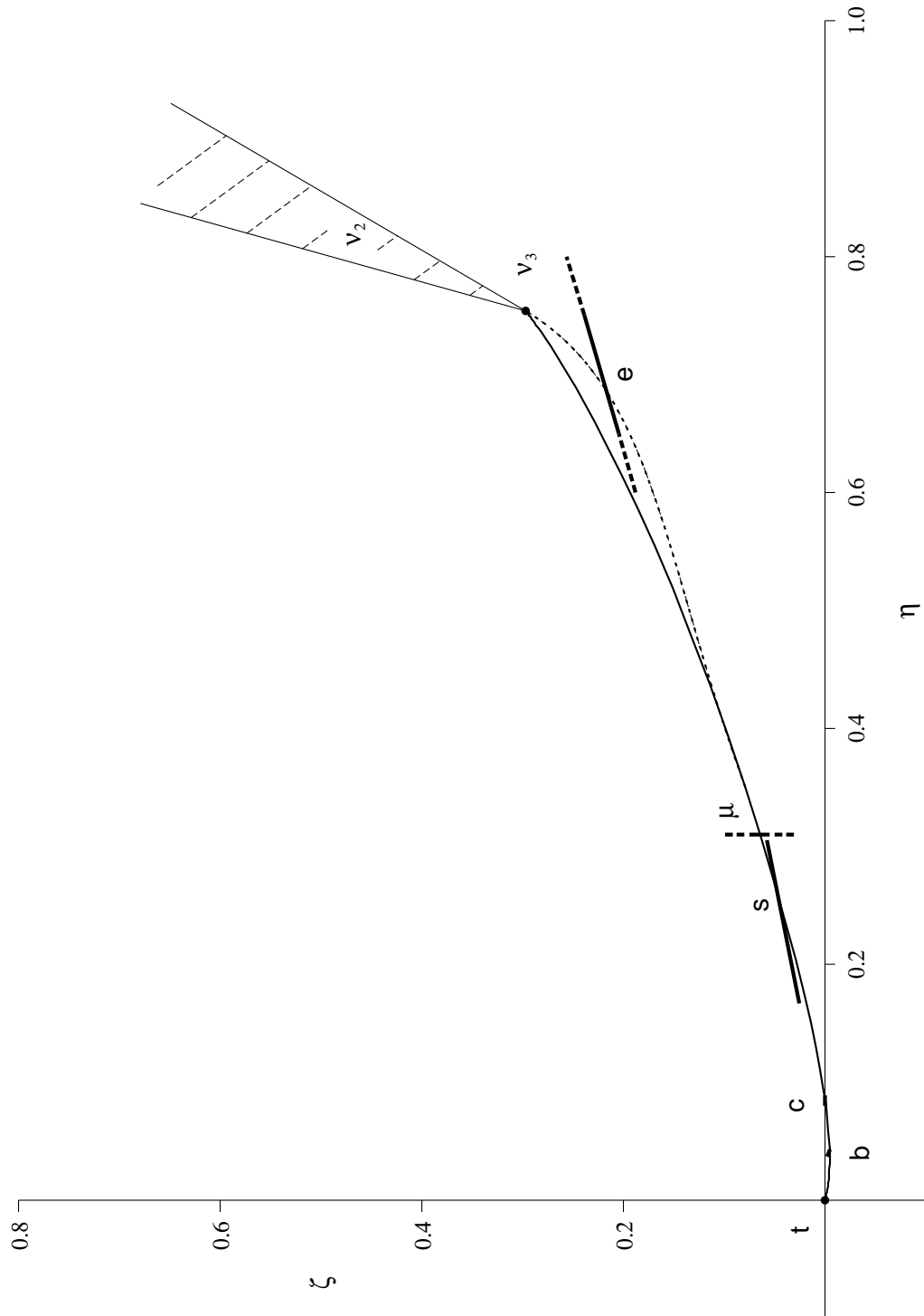


Figure 5: Projection of Figure 4 onto the  $\eta\zeta$ -plane. The full curve represents the DSM one-loop calculation of [5] and the dashed curve its suggested deformation at low scales to fit the data on  $m_e$  and  $U_{e2}$ .

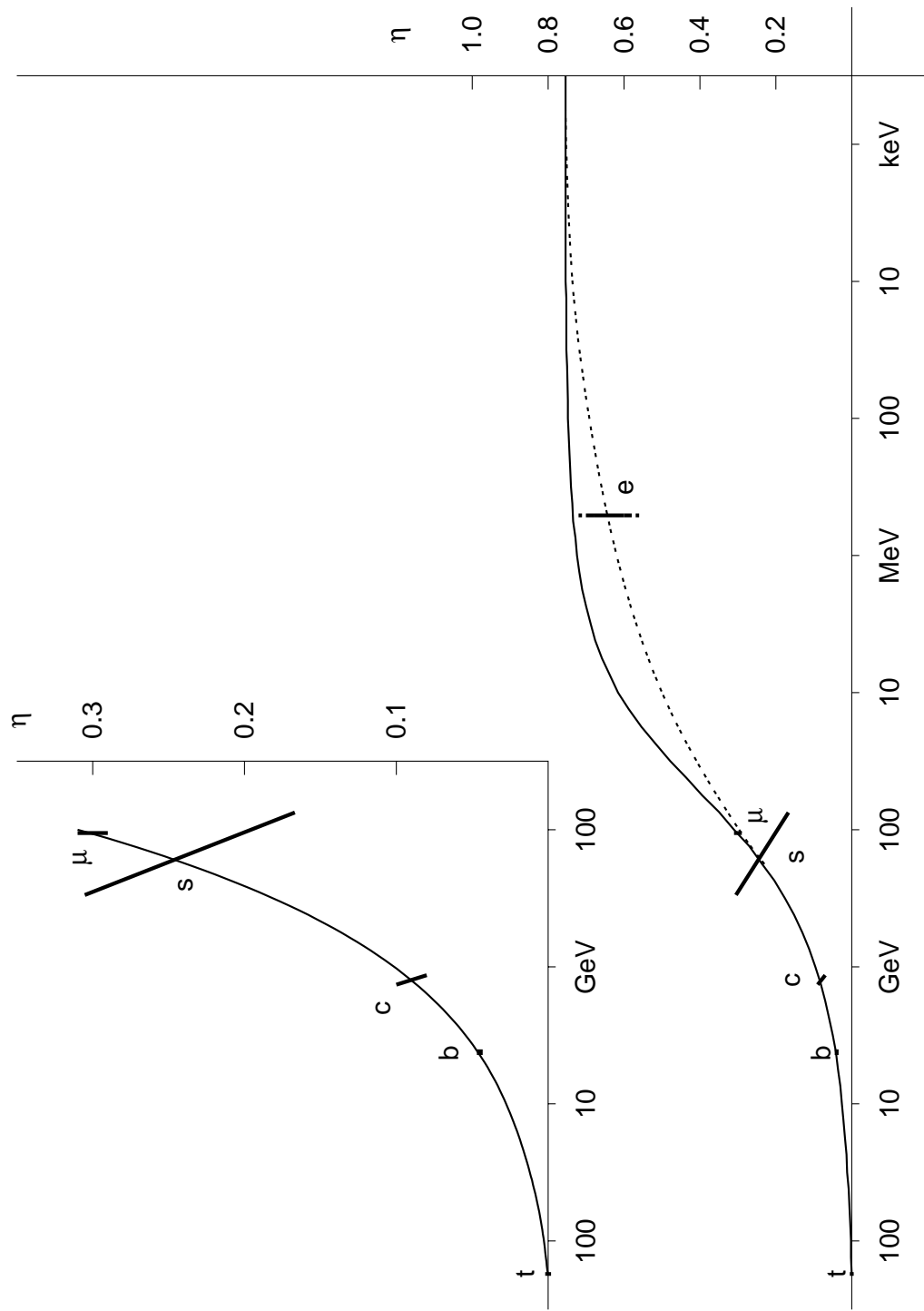


Figure 6: Projection of Figure 4 onto the  $\mu\eta$ -plane. The full curve represents the DSM one-loop calculation of [5] and the dashed curve its suggested deformation at low scales to fit the data on  $m_e$  and  $U_{e2}$ .

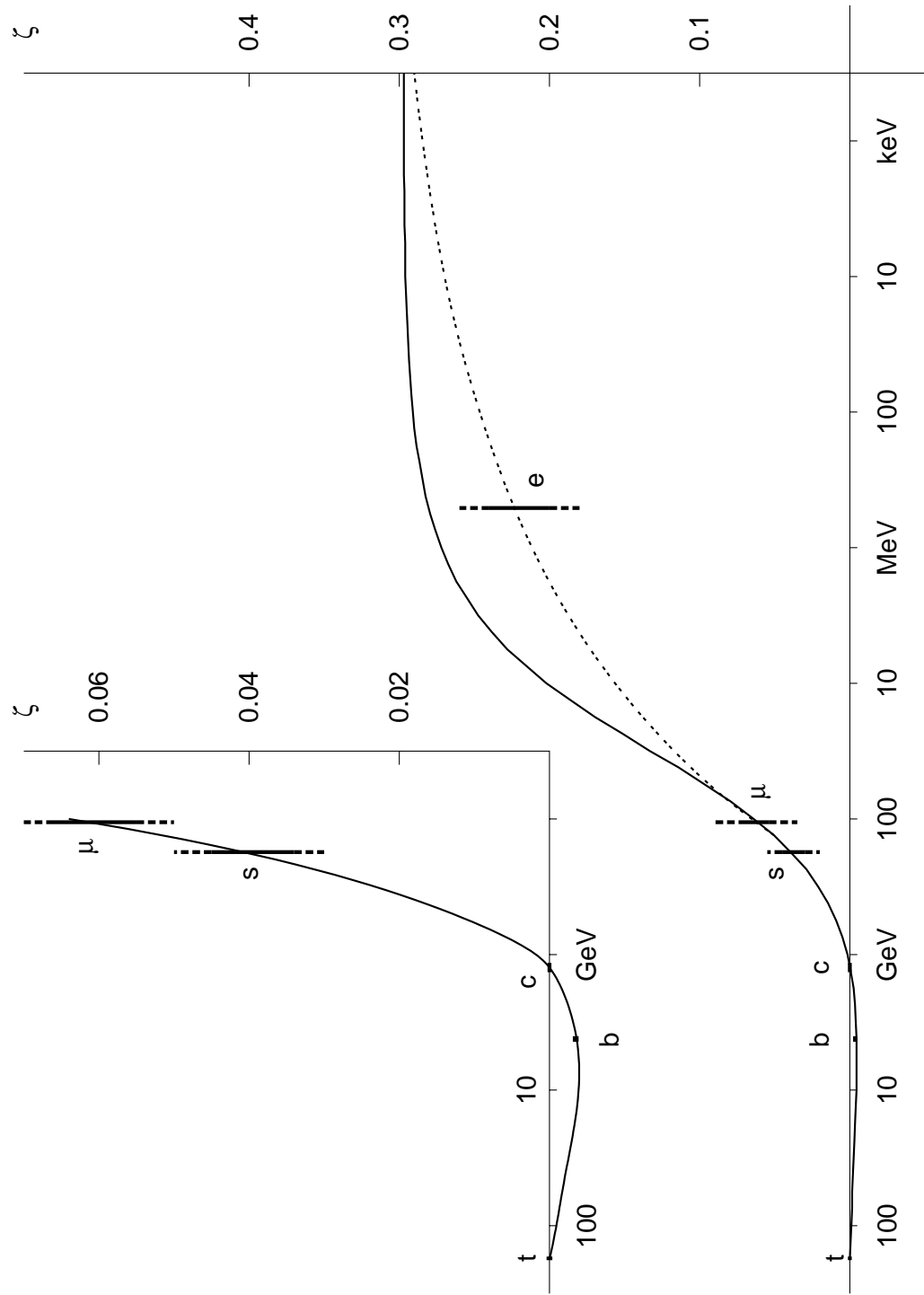


Figure 7: Projection of Figure 4 onto the  $\mu\zeta$ -plane. The full curve represents the DSM one-loop calculation of [5] and the dashed curve its suggested deformation at low scales to fit the data on  $m_e$  and  $U_{e2}$ .

The range of values for  $m_s$  is given in [4] as 75—170 MeV, and in [6] as 100—300 MeV, depending on the scale at which the limits were determined respectively. The allowed region shown for  $\mathbf{r}(m_s)$  in Figure 4 corresponds to the union of the above two ranges for  $m_s$  values, which allowed region, one will notice, does not lie entirely on the plaquette corresponding to an  $m_s$  value at 176 MeV but protrudes to either side of it. This gives then a 4th point on the trajectory for  $\mathbf{r}(\mu)$ . As noted before, given the present errors on the CKM matrix elements, there is actually an alternative solution for  $\mathbf{v}_s$  with a different sign for the third component to that given in (6), which would imply a corresponding change in sign for  $\mathbf{r}(m_s)$  in Figure 4. This alternative we disfavour since it would lead to a trajectory for  $\mathbf{r}(\mu)$  less smooth than given by the above solution and shall be ignored for the present.

The above represents more or less the most that can be extracted from the data on quark masses and mixing (barring CP violation) about the rotating vector  $\mathbf{r}(\mu)$  apart from some as yet rather uncertain information from the masses of the light quarks  $u$  and  $d$ . The method we used for extracting the fermion masses from the “leakage mechanism” as contained in e.g. (1) was meant only for freely propagating particles and should not in principle be applied to quarks which are confined, except approximately to the heavier quarks which are generally regarded as quasi-free. For the light quarks  $u$  and  $d$  which are tightly confined, it is clearly not applicable. The question then arises in what way these light quark masses are to be defined. Experimentally, these masses are determined at some convenient but somewhat arbitrary scale such as 1 or 2 GeV, and it is not clear what these values should correspond to in the “leakage mechanism”. One possibility is to consider these mass values as the “leakage” from the rotating vector  $\mathbf{r}(\mu)$  taken at the chosen scale 1 or 2 GeV into the vectors  $\mathbf{v}_u$  and  $\mathbf{v}_d$  thus:

$$|\mathbf{v}_u \cdot \mathbf{r}(\mu)|^2 \stackrel{?}{=} m_u/m_t; \quad |\mathbf{v}_d \cdot \mathbf{r}(\mu)|^2 \stackrel{?}{=} m_d/m_b. \quad (11)$$

In that case one obtains values for both  $m_u$  and  $m_d$  of the right order of magnitude in the MeV region, but it is not certain whether this is of much significance. As matters stand, therefore, we can only leave open the question of the light quark masses.

### 3 Extracting $\mathbf{r}(\mu)$ from lepton data

To proceed further, one turns now to the leptons for which the preceding analysis for quarks can in principle be independently repeated, for as far as

the premises of the rotating mass matrix as set up at the beginning of this paper is concerned, there is strictly nothing which needs connect the mass matrices of quarks and leptons. However, the DSM scheme suggests that the rotating matrices for quarks and leptons both lie on the same trajectory, the last being specified just by the vev's of the (dual colour) Higgs fields which are independent of the fermion type [7, 5], and this suggestion has been borne out by an analysis directly on the data done in the planar approximation [3]. It makes practical sense therefore to adopt the same position here, especially since it raises the stakes and makes the present analysis an even more stringent test for the rotation hypothesis. This means in particular that the state vector, say  $\mathbf{v}_\tau$ , of the  $\tau$  lepton, this being the heaviest eigenstate of the lepton mass matrix, could be identified with again the vector  $\mathbf{r}(\mu)$  taken at the scale  $\mu = m_\tau$ , the location of which can readily be determined by interpolating  $\mathbf{r}(\mu)$  between  $m_b$  and  $m_c$ , as in Figure 3.

Having fixed  $\mathbf{v}_\tau$ , one can constrain the vector  $\mathbf{r}(\mu)$  at  $\mu = m_\mu$  by the condition:

$$|\mathbf{r}(m_\mu) \cdot \mathbf{v}_\mu|^2 = m_\mu/m_\tau, \quad (12)$$

with:

$$\mathbf{v}_\mu \cdot \mathbf{v}_\tau = 0, \quad (13)$$

or in other words:

$$1 - |\mathbf{r}(m_\mu) \cdot \mathbf{v}_\tau|^2 = m_\mu/m_\tau. \quad (14)$$

This gives 4 solutions for  $\eta(m_\mu), \zeta(m_\mu)$ , corresponding to respectively the two signs of  $\mathbf{r}(m_\mu) \cdot \mathbf{v}_\tau$  and the two signs of  $\xi(m_\mu) = \pm \sqrt{1 - \eta(m_\mu)^2 - \zeta(m_\mu)^2}$ . These 4 solution are, however, widely separated, so that there is no ambiguity in discarding 3 of them by continuity. Indeed, the 2 solutions with  $\xi(m_\mu)$  negative can thus be discarded, the value for  $\xi(\mu)$  being so far always large and positive, and so can also the solution with  $\mathbf{r}(m_\mu) \cdot \mathbf{v}_\tau$  negative which will take  $\mathbf{r}(m_\mu)$  far into another quadrant of the plot. This leaves then the solution shown in Figure 4 which, by inputting the empirical values of  $m_\tau = 1777$  MeV and  $m_\mu = 105$  MeV taken from [4], gives as the allowed region for  $\mathbf{r}(m_\mu)$  a narrow band on the  $\mu$  plaquette approximately parallel to the  $\zeta$ -axis, the width of the band representing the error on  $\mathbf{v}_\tau$  obtained from the above interpolation. For the rotation hypothesis to be valid, the trajectory for  $\mathbf{r}(\mu)$  is required to pass through this band at  $\mu = m_\mu$ .

The above information on the vector  $\mathbf{r}(m_\mu)$  determines also to a fair approximation the state vector  $\mathbf{v}_\mu$ , the latter being constrained by the “leakage” mechanism to lie on the plane containing  $\mathbf{v}_\tau$  and  $\mathbf{r}(m_\mu)$  and to be orthogonal

to  $\mathbf{v}_\tau$ . That this is so can be seen as follows. As noted already, the vector  $\mathbf{v}_\tau$  being near the vector  $\mathbf{r}(m_c)$  and therefore lying very nearly on the  $\xi \eta$ -plane, the allowed band for  $\mathbf{r}(m_\mu)$  defined by (14) is very nearly parallel to the  $\zeta$ -axis so that the second component of  $\mathbf{r}(m_\mu)$ , namely  $\eta(m_\mu)$ , is very well determined, as is depicted in Figure 6. By interpolating with a curve drawn through the four quite accurate points for respectively  $t, b, c$  and  $\mu$ , one can then get a fair estimate for the value of  $\eta(m_s)$ . Hence from Figure 5, one can read off the corresponding value for the third component  $\zeta(m_s)$  which on insertion into Figure 7 then allows for an extrapolation to the  $\mu$  mass scale to give an estimate for the value of  $\zeta(m_\mu)$ , which though rough, being in any case small, is sufficient for our purpose. Having then obtained the vector  $\mathbf{r}(m_\mu)$ , the state vector of  $\mu$ , namely  $\mathbf{v}_\mu$ , is also determined by the conditions stated at the beginning of the paragraph. At the same time, of course, the state vector  $\mathbf{v}_e$  of  $e$  is also determined by orthogonality to both  $\mathbf{v}_\mu$  and  $\mathbf{v}_\tau$ . The actual numerical values we so obtained for the charged leptonic triad which we shall use later for our analysis are as follows:

$$\begin{aligned}\mathbf{v}_\tau &= (0.9975, 0.0700, -0.0015), \\ \mathbf{v}_\mu &= (-0.0654, 0.9516, 0.3003), \\ \mathbf{v}_e &= (0.0224, -0.2995, 0.9538).\end{aligned}\tag{15}$$

This determination of the charged lepton triad on which the analysis in the remainder of this section depends is about the best that one can do for the moment but is obviously not as accurate as one could wish. Nevertheless, as we shall see, it still serves its purpose in allowing us to extract some interesting information on  $\mathbf{r}(\mu)$  for the low  $\mu$  region.

First, according to the “leakage mechanism”, the mass of the electron is given by:

$$|\mathbf{r}(m_e) \cdot \mathbf{v}_e|^2 = m_e/m_\tau,\tag{16}$$

which, as for (12) and for the same reasons, gives 4 solutions, 2 of which, namely those corresponding to negative values for  $\xi(m_e)$ , can easily be discarded by continuity arguments, leaving two which are represented in Figure 4 by respectively the line drawn on the  $e$ -plaquette and another line (not shown) nearly parallel to the first but 0.035 units lower (and hence almost coinciding with the one shown). Again, for the rotation hypothesis to be valid, the trajectory for  $\mathbf{r}(\mu)$  has to pass through one of these 2 line at  $\mu = m_e$ . In obtaining these lines, we have of course input the well known value of 0.51 MeV for the mass of the electron.

Secondly, the MNS [8] lepton mixing matrix elements  $U_{\mu 3}$  and  $U_{e 3}$ , as studied in oscillation experiments on respectively atmospheric neutrinos [9, 10] and reactor neutrinos such as [11], are given just by the inner products:

$$U_{\mu 3} = \mathbf{v}_\mu \cdot \mathbf{v}_3, \quad (17)$$

and:

$$U_{e 3} = \mathbf{v}_e \cdot \mathbf{v}_3, \quad (18)$$

with  $\mathbf{v}_3 = \mathbf{r}(m_{\nu_3})$  being the state vector of the heaviest neutrino  $\nu_3$ . With the  $\mu$  state vector as determined above in (15), one obtains by inputting the experimental range for  $|U_{\mu 3}|^2$  of about 1/3 to 2/3 [9, 10] again four solutions for the allowed region, three of which are easily discarded by continuity arguments, leaving one (corresponding to  $U_{\mu 3}$  and  $\xi(m_{\nu_3})$  both positive) which is represented in Figure 4 by the area bounded by the two near vertical lines on the  $\nu_3$ -plaquette. Similarly, with the  $e$  state vector as determined in (15), one obtains by inputting the experimental bound  $|U_{e 3}|^2 < 0.027$  [11], four solutions for the allowed region, but this time only two (corresponding to  $\xi(m_{\nu_3})$  negative) can be discarded, the other two being adjacent merge into one as represented in Figure 4 by the area bounded by the two near horizontal lines on the  $\nu_3$ -plaquette. The consequent allowed region for the vector  $\mathbf{r}(m_{\nu_3})$  is thus represented by the roughly rectangular area shown, where we have put  $m_{\nu_3}^2 \sim 3 \times 10^{-3} \text{ eV}^2$  as preferred by [9, 10] and [12].

Finally, the mixing element  $U_{e 2}$  as inferred from solar neutrino experiments is given as:

$$U_{e 2} = \mathbf{v}_e \cdot \mathbf{v}_2, \quad (19)$$

where  $\mathbf{v}_2$  is the state vector for the second heaviest neutrino  $\nu_2$  which is by definition orthogonal to  $\mathbf{v}_3$ . Following thus the same procedure as in the preceding paragraph, one can determine the allowed region for the vector  $\mathbf{v}_2$  by inputting the bounds on  $\mathbf{v}_3$  as obtained above and the experimental bounds on  $U_{e 2}$  [9, 13, 14]. However, to extract  $\mathbf{r}(m_{\nu_2})$  from this, one would need  $m_{\nu_2}$  which is experimentally still largely unknown so that the above information on  $\mathbf{v}_2$  cannot readily be presented in Figure 4. But, as we shall see, there is another way of displaying this information.

## 4 Discussion

The allowed regions for the vector  $\mathbf{r}(\mu)$  for various scales  $\mu$  deduced in the preceding two sections and displayed in Figure 4 and its projections Figures 5–7 represent all the information that can be extracted at present from

fermion mass and mixing parameters, apart from the  $u, d$  masses and the solar neutrino angle  $U_{e2}$  already noted. If the rotation hypothesis set out at the beginning is to be valid, then all the allowed regions should line up along some smooth 3-D curve from the heaviest  $t$  to the lowest  $\nu_3$ . This is seen in the above-quoted figures to be indeed the case. In the high energy region, say down to the  $\mu$  mass scale, where the allowed regions are mostly small, the alignment is seen to be quite accurate, not only in the projection of Figure 6 on to the  $\mu\eta$ -plane as already noted in [3], but also in the two other directions as seen in Figures 5 and 7. Below the  $\mu$  mass scale, the allowed regions are larger and the constraints not too stringent but they are seen still to be thoroughly consistent with alignment on a smooth trajectory spanning some 13 orders of magnitude in energy. This looks to us nontrivial and lends direct empirical support to the rotation hypothesis without any theoretical input other than those stated at the beginning of this paper. Besides, this gives us a rough outline of the rotation curve should it exist. In particular, we note from e.g. Figures 6 and 7 that  $\mathbf{r}(\mu)$  seems to approach asymptotic limits, i.e. rotational fixed points, for both  $\mu \rightarrow \infty$  and  $\mu \rightarrow 0$ .

On the other hand, the DSM scheme, in which context the idea of rotation giving rise to the fermion mass hierarchy and mixing was first suggested, proposed a perturbative method for calculating the rotation trajectory [7] which has been carried out so far to 1-loop order. The calculation done already a few years ago [5] with the 3 parameters in the model fitted to the mass ratios  $m_c/m_t$ ,  $m_\mu/m_\tau$  and to the Cabibbo angle is reproduced in Figures 4–7. Although this result has never been explicitly presented before, it can be inferred from e.g. Figure 3 of [5] and transformed to the present frame (4) from the frame used there through the vectors:

$$\begin{aligned}\mathbf{v}_t &= (0.9999, 0.0117, 0.0008); \\ \mathbf{v}_c &= (-0.0110, 0.9148, 0.4038); \\ \mathbf{v}_u &= (0.0040, -0.4038, 0.9149)\end{aligned}\tag{20}$$

obtained from the previous calculation [5]. It is seen to agree very well with the newly extracted information down to the  $\mu$  mass scale. In particular, the rotational fixed point predicted by the DSM at  $\mu = \infty$  is seen to be fully consistent with the data. Below the  $\mu$  mass the DSM curve calculated to 1-loop order begins to deviate from the regions allowed by experiment. For example, on the  $e$ -plaquette in Figure 4, the DSM curve if exact should hit the allowed line at  $\mu = m_e$  but, as indicated by the little cross, it hits the plaquette instead at some distance from the allowed line. This deviation

represents the difference in the mass of the electron as predicted by the old calculation [5] from its true value, i.e. 6 MeV instead of 0.51 MeV. Such a deviation is of course expected, since at lower scales, the vector  $\mathbf{r}(\mu)$  moves further and further from the high energy fixed point predicted by the scheme so that the 1-loop calculation for the trajectory will become less and less reliable. However, the 1-loop approximate trajectory from [5] still hits the  $\nu_3$  plaquette inside the allowed region, in other words giving correct predictions for the MNS mixing elements  $U_{\mu 3}$  and  $U_{e 3}$ . This is because these elements depend only on the vector  $\mathbf{v}_3 = \mathbf{r}(m_{\nu_3})$  which, as indicated in Figures 6 and 7, is already near the asymptotic value. Hence, the fact the the calculation agrees with data for  $U_{\mu 3}$  and  $U_{e 3}$  suggests that the rotational fixed point at  $\mu = 0$  is correctly predicted, although the rotational curve itself near this fixed point is not, by the 1-loop approximation.

In contrast, the state vector  $\mathbf{v}_2$  of the second heaviest neutrino  $\nu_2$  represents the tangent vector to the trajectory near the low energy fixed point and cannot therefore be expected to be accurately predicted by the 1-loop calculation of [5]. Indeed, the value predicted by [5] for the mixing element  $U_{e 2}$  which depends on  $\mathbf{v}_2$  fell outside the limits set by the solar neutrino experiments. In our present analysis, the information on  $\mathbf{v}_2$  extracted from the experimental limits on  $U_{e 2}$  can be presented as a wedge-shaped region in Figure 5 in which the tangent to the trajectory at the low energy fixed point is supposed to lie, which region is estimated with a bound  $|U_{e 2}|^2 \sim 0.33 \pm 0.1$  favoured by present experiments [9, 13]. As can be seen in the figure, the trajectory predicted by the DSM 1-loop calculation does not satisfy this criterion. Again, as in previous cases, there are in fact four solutions to this allowed region, among which we have chosen to display the one which is nearest to accommodating the DSM 1-loop trajectory. However, this is not surprising since it is already expected that the 1-loop trajectory will be unreliable below the  $\mu$  mass scale. In that case, it may be interesting turning the argument around to use the information at low scale, scanty though it is at present, to constrain the exact trajectory if such really exists. One sees then that just by deforming somewhat the 1-loop curve, one would be able to remove both the previously noted discrepancies in the  $e$  mass and in the mixing element  $U_{e 2}$ , as indicated in Figures 5, 6 and 7.

In summary, we conclude that the existing data on fermion mass and mixing when appropriately interpreted do support the hypothesis of a mass matrix rotating with changing scales, and that the rotation trajectory indicated bears a close resemblance to that predicted earlier by the DSM scheme.

We thank Carmen Garcia Garcia for kindly helping us with the best fit to

the data presented in Figure 3, and Bill Scott for advising us on the neutrino oscillation data.

## References

- [1] N. Cabibbo, Phys. Rev. Lett. **10**, 531 (1963); M. Kobayashi and T. Maskawa, Prog. Teor. Phys. 49, 652 (1973).
- [2] See e.g. Chan Hong-Mo hep-th/0007016, Int. J. Mod. Phys. A16, 163, (2001), and/or Chan Hong-Mo and Tsou Sheung Tsun, hep-ph/0008312 (2000), Proc. 8th Asia-Pacific Phys. Conf. APPC 2000, ed. Yeong-Der Yao et al. (World Scientific, Singapore 2001) p. 447.
- [3] José Bordes, Chan Hong-Mo and Tsou Sheung Tsun, hep-ph/0104036 (2001).
- [4] Review of Particle Physics, D.E. Groom et al., Eur. Phys. Journ. C15 (2000) 1.
- [5] José Bordes, Chan Hong-Mo and Tsou Sheung Tsun, hep-ph/9901440, Eur. Phys. J. C 10, 63, (1999).
- [6] R. M. Barnett et. al, Phys. Rev. D54, 1 (1996).
- [7] José Bordes, Chan Hong-Mo, Jacqueline Faridani, Jakov Pfaudler, and Tsou Sheung Tsun, Phys. Rev. D58, 013004, (1998), hep-ph/9712276.
- [8] Z. Maki, M. Nakagawa and S. Sakata, Progr. Theor. Phys. 28, 870 (1962).
- [9] Superkamiokande data, see e.g. talk by T. Toshito at ICHEP'00, Osaka (2000).
- [10] Soudan II data, see e.g. talk by G. Pearce, at ICHEP'00, Osaka (2000).
- [11] CHOOZ collaboration, M. Apollonio et al., Phys. Lett. B466, 415, (1999), hep-ex/9907037.
- [12] S.H. Ahm et al., Phys. Lett. B511 (2001) 178, hep-ex/0103001.
- [13] Q.R. Ahmad et al., Phys. Rev. Lett. 87 (2001) 071301, nucl-ex/0106015.
- [14] G.L. Fogli et al., hep-ph/0106247, Phys. Rev. D64, 0093007 (2001).